

Mechanical stabilization of the Levitron's realistic model

Arturo Olvera^{1,a}, Abraham De la Rosa¹, and Claudia M Giordano²

¹ IIMAS-UNAM 04510 Mexico, D.F. Mexico

² Instituto de Astrofísica de La Plata, Facultad de Ciencias Astronómicas y Geofísicas – UNLP Paseo del Bosque, B1900FWA La Plata, Argentina

Received 15 January 2016 / Received in final form 6 April 2016

Published online XX XX 2016

Abstract. The stability of the magnetic levitation showed by the Levitron was studied by M.V. Berry as a six degrees of freedom Hamiltonian system using an adiabatic approximation. Further, H.R. Dullin found critical spin rate bounds where the levitation persists and R.F. Gans et al. offered numerical results regarding the initial conditions' manifold where this occurs. In the line of this series of works, first, we extend the equations of motion to include dissipation for a more realistic model, and then introduce a mechanical forcing to inject energy into the system in order to prevent the Levitron from falling. A systematic study of the flying time as a function of the forcing parameters is carried out which yields detailed bifurcation diagrams showing an Arnold's tongues structure. The stability of these solutions were studied with the help of a novel method to compute the maximum Lyapunov exponent called MEGNO. The bifurcation diagrams for MEGNO reproduce the same Arnold's tongue structure.

1 Introduction

The Levitron is a mechanical device conformed basically by two parts: the top, a magnetized rotationally symmetric rigid body of uniform mass that behaves as a magnetic dipole, and the base that provides a permanent magnetic field such that the interaction with the magnetic dipole compensates the gravitational force acting on the top when put to spin over it.

Magnetic levitation of spinning bodies was discovered by Roy Harrigan who developed a device using a square magnetic base and by calibrating the volume and mass of a magnetic top he achieved the inertial and magnetic momenta leading to its persistent magnetic levitation. The Earnshaw's theorem [1] establishes the rules for the magnetic levitation of static dipoles, where no stable configuration of static dipoles is possible, leaving the Levitron's dynamics to be understood.

^a e-mail: aoc@mym.iimas.unam.mx

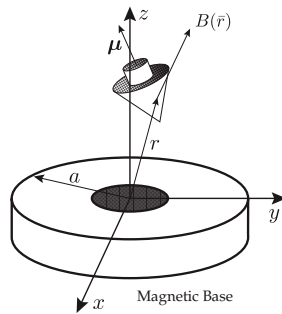


Fig. 1. Diagram of the Levitron TM: $B(\vec{r})$ is the static magnetic field of the base and μ is the top magnetic dipole

35 Many different attempts to comprehend how the Levitron's mechanism works have
 36 been done. In fact, B. Hones in 1995 was among the firsts to address the study of
 37 the Levitron; however, his discussion did not allow for levitation over a circular mag-
 38 netic base which is indeed possible. The more theoretical approaches to explain the
 39 dynamics of this device were made principally by [2] and [3] in 1996. A Hamiltonian
 40 formulation of six degrees of freedom and an adiabatic theory to prove that the mag-
 41 netic levitation is possible only for some ranges of the spinning rates is given in [2].
 42 Therein the role of the precession movement of the top to allow persisting levitation
 43 is also shown. In [3] both physical and numerical experiments were performed to con-
 44 firm the theoretical results of M.V. Berry. Later on, in [4], the Hamiltonian approach
 45 was further developed by studying the local behavior near an equilibrium point of
 46 the system, to find invariant regions in the phase space where persistent levitation of
 47 the top is feasible.

48 The results presented in [4] are very useful for the numerical analysis of the equa-
 49 tions. Also, in [5] dimensionless constants that facilitate the the analysis of simula-
 50 tions are introduced. Both papers follow the guideline drew by [2] and are the base for
 51 the present work. Nevertheless none of the cited papers have studied the Levitron's
 52 dynamics considering energy losses caused by friction, in [6] we can find a first at-
 53 tempt to introduce losses in the dynamic of the Levitron.

54 The aim of this effort is to present a numerical study of the Levitron's dynam-
 55 ics. For the sake of completeness and clarity the equations of motion are included,
 56 and invariant regions in phase space as well as equilibrium states are described. A
 57 numerical verification of the range for the spinning rates given in [2] is performed, a
 58 persistent levitation of the top being observed. Then, dissipative terms are introduced
 59 in the equations of motion to model the friction with the air in a more realistic set-
 60 ting resulting finite flight times. Since the system with dissipative terms is no longer
 61 Hamiltonian, a strategy to inject energy into the system is proposed, which will be
 62 numerically explored studying the possibility to counteract the effect of dissipation
 63 preventing the top to fall down. It should be pointed out that this approach is of a
 64 mechanical nature, that is, no electromagnetic drive [6] or air jet propulsion [3] are
 65 considered. This scheme corresponds to a mechanical perturbation of the position of
 66 the magnetic base using a parametric excitation.

67 Furthermore a proper method for computing the Lyapunov exponents is chosen to
 68 study the stability of the solutions of the more complex equations of motion, includ-
 69 ing both dissipation and perturbation terms. These equations are numerically studied
 70 over a grid in the perturbation parameter space to determine the regions where max-
 71 imum times of flight are observed. In a similar way the stability of the numerical
 72 solutions are also studied. The final section is devoted to present the conclusions of
 73 the overall analysis.

74 2 Equations of motion

75 In order to obtain the equations of motion of the Levitron, we follow the scheme
76 delivered in [5] where the magnetic base is modelled as a ring dipole of radius a , the
77 magnetic potential along the vertical axis being

$$V_0(z) = \frac{M}{2} \frac{za}{(a^2 + z^2)^{3/2}}. \quad (1)$$

78 The magnetic field $B(\bar{r}) = -\nabla V(\bar{r})$ is defined by the magnetic potential

$$V(\bar{r}) = \Phi_0 - \frac{\rho^2}{4} \Phi_2(z) \pm \dots, \quad \text{where} \quad \Phi_k(z) = \frac{d^k}{dz^k} V_0(z). \quad (2)$$

79 Finally, the potential energy of the Levitron is given by the gravitational component
80 and the magnetic interaction of the top with the magnetic field (see [7] for details)

$$\Psi(\bar{r}, \mathbf{R}) = mgz - \langle B(\bar{r}), \boldsymbol{\mu} \rangle, \quad (3)$$

81 where $\boldsymbol{\mu} = \mu \mathbf{R} e_z$ is the magnetic momentum of the Levitron in the external reference
82 frame, \mathbf{R} being a rotational matrix.

83 Meantime, the kinetic energy is given by the model of the eulerian top (see [8]
84 and [5]).

For the sake of convenience we will deal with the dimensionless equations of motion
of the spinning top, by scaling by the length a (the radius of the dipole ring) and a
consistent time scale τ . Therefore we define

$$x = aX, \quad y = aY, \quad z = aZ, \quad t = (a/g)^{1/2} \tau.$$

85 By (2) and (1), V can be written in terms of the dimensionless variables as

$$V = \frac{M_e}{4\pi a^2} [f_0(Z) + (X^2 + Y^2)f_2(Z) + O((X^2 + Y^2)^2)] =: \frac{M_e}{4\pi a^2} \Phi, \quad (4)$$

86 with

$$f_0(Z) = \frac{Z}{(1 + Z^2)^{3/2}}, \quad f_2(Z) = -\frac{3(2Z^2 - 3)Z}{4(1 + Z^2)^{7/2}} \quad (5)$$

87 where $M_e = 2\pi Ma$ is the net strength of the dipoles of the ring and a is the effective
88 radius.

89 The Hamiltonian proposed in [5] is

$$\mathcal{H} = \frac{1}{2} \left(p_X^2 + p_Y^2 + p_Z^2 + \frac{p_\theta^2}{A} + \frac{[p_\psi - p_\phi \cos \theta]^2}{A \sin^2 \theta} + \frac{p_\phi^2}{C} \right) \\ - \mathcal{M} \left[\sin \theta \left(\cos \psi \frac{\partial \Phi}{\partial X} + \sin \psi \frac{\partial \Phi}{\partial Y} \right) + \cos \theta \frac{\partial \Phi}{\partial Z} \right] + Z,$$

90 and the concomitant equations of motion read

$$\dot{X} = p_X \quad (6a)$$

$$\dot{Y} = p_Y \quad (6b)$$

$$\dot{Z} = p_Z \quad (6c)$$

$$\dot{\theta} = \frac{p_\theta}{A} \quad (6d)$$

$$\dot{\psi} = \frac{p_\psi - p_\phi \cos \theta}{A \sin^2 \theta} \quad (6e)$$

$$\dot{\phi} = -\cos \theta \cdot \frac{p_\psi - p_\phi \cos \theta}{A \sin^2 \theta} + \frac{p_\phi}{C} \quad (6f)$$

$$p_{\dot{X}} = 2\mathcal{M} [f_2(Z) \sin \theta \cos \psi + X f_2'(Z) \cos \theta] \quad (6g)$$

$$p_{\dot{Y}} = 2\mathcal{M} [f_2(Z) \sin \theta \sin \psi + Y f_2'(Z) \cos \theta] \quad (6h)$$

$$p_{\dot{Z}} = \mathcal{M} [2f_2'(Z) \sin \theta (X \cos \psi + Y \sin \psi) + \cos \theta (f_0''(Z) + (X^2 + Y^2) f_2''(Z))] - 1 \quad (6i)$$

$$p_{\dot{\theta}} = -\frac{(p_\phi \cos \theta - p_\psi)(p_\psi \cos \theta - p_\phi)}{A \sin^3 \theta} + \mathcal{M} [2f_2(Z) \cos \theta (X \cos \psi + Y \sin \psi) - \sin \theta (f_0'(Z) + (X^2 + Y^2) f_2'(Z))] \quad (6j)$$

$$p_{\dot{\psi}} = 2\mathcal{M} f_2(Z) \sin \theta (Y \cos \psi - X \sin \psi) \quad (6k)$$

$$p_{\dot{\phi}} = 0 \quad (6l)$$

91 where

$$A = \frac{\Theta_1}{ma^2}, \quad C = \frac{\Theta_2}{ma^2}, \quad \mathcal{M} = \frac{-\mu M_e}{4\pi m g a^4}, \quad (7)$$

92 are positive constants, Θ_1 and Θ_2 are the inertial moments of the top, m is the mass
93 and M_e is the net strength of the dipoles of the ring. Of course \mathcal{H} is a conserved
94 quantity as well as p_ϕ .

95 We want to remark that the kinetic energy of our hamiltonian function \mathcal{H} is
96 defined with the eulerian angular coordinates such that $\theta = 0$ is a singular value. In
97 [6,9] and [4], they use a different set of angular coordinates where $\theta = 0$ is now a
98 regular value of the kinetic energy.

Following the ideas in [4], it can be seen that

$$Inv = \{X = Y = 0, \theta = 0, p_X = p_Y = 0, p_\theta = 0, p_\psi = p_\phi\}$$

99 is an invariant set of the equations of motion. The corresponding Hamiltonian
100 function is

$$\mathcal{H}_{Inv} = \frac{1}{2} \left(p_Z^2 + \frac{p_\phi^2}{C} \right) - \mathcal{M} \left[\frac{\partial \Phi}{\partial Z} \right] + Z. \quad (8)$$

101 The dynamics in this region is given by

$$\dot{Z} = p_Z \qquad \dot{p}_Z = \mathcal{M}f_0''(Z) - 1 \qquad (9)$$

$$\dot{\phi} = \frac{p_\phi}{C} = \sigma \qquad \dot{p}_\phi = 0 \qquad (10)$$

102 This system has two fixed points which are defined by the relationship

$$f_0''(Z) = \frac{1}{\mathcal{M}}. \qquad (11)$$

103 In [5] the authors adopt $\mathcal{M} = 8.187957392$ and the stable fixed point is
 104 $Z_c = 1.693848849$. The linearized system of (9) near the point $(Z_s, 0)$ is a
 105 harmonic oscillator:

$$\ddot{Z} + V_{Inv}''(Z_s)Z = 0, \qquad (12)$$

106 where

$$V_{Inv} = -\mathcal{M}f_0'(Z) + Z. \qquad (13)$$

Thus, in the invariant region, Z oscillates with the frequency

$$\sqrt{-\mathcal{M}f_0'''(Z_s)}.$$

107 A similar kind of linear equation was found by [3].

108 3 Numerical analysis

To integrate the system (6), we fix the parameters A and C as in [5], namely

$$A = 0.089, \qquad C = 0.139.$$

109 These values correspond to physical measurements, the effective radius being
 110 $a = 34.7$ mm. The value of a determines the inertial momenta of the spinning top.

111 We adopt the value $\mathcal{M} = 8.188$ for which the two equilibrium points of the lin-
 112 earized system are equal.

113 The numerical method we have chosen to cope with the integration in regions of
 114 phase space where the system can become stiff is a Runge-Kutta-Fehlberg 7–8.

The Eqs. (6e), (6f) and (6j) are singular whenever $\theta = 0$ or π . To overcome
 this issue we control the numerators of such expressions. For instance, in the case of
 Eq. (6e) we fix to zero the entry of the field corresponding to ψ whenever it is

$$|p_\psi - p_\theta \cos \theta| \leq tol.$$

115 The same control is kept in the other two equations. The value of tol is calibrated
 116 numerically, not having found any significant difference for values lesser than 0.0001.
 117 We verify that to have a stable flight of the spinning top p_ϕ and p_ψ should be close;
 118 also in this case our control makes sense. Let us notice that the obtained results
 119 confirm the ones in [2].

120 Finally, the initial conditions have been picked up close to the equilibrium point
 121 Z_c associated to $\mathcal{M} = 8.188$.

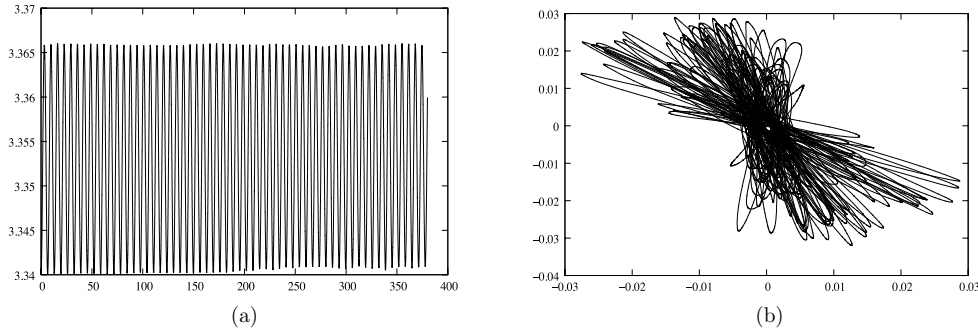


Fig. 2. (a) Time evolution of z -coordinate; (b) (x, y) -coordinates.

122 3.1 Non symmetric solution

123 In [5], the authors propose a symmetric solution of the system with small precession,
 124 explicitly

$$\mathbf{q} = (r \cos \Omega t, r \sin \Omega t, h, \alpha, \Omega t, w t)^T$$

$$\mathbf{p} = [-r\Omega \sin \Omega t, r\Omega \cos \Omega t, 0, 0, \Omega(A \sin^2 \alpha + C \cos^2 \alpha) + Cw \cos \alpha, C(w + \Omega\alpha)]^T,$$

125 where the spinning velocity w can be fixed freely and then we can find the values of
 126 r , α , h and Ω .

127 In the case where p_ϕ and p_ψ are different but very close to each other, we take
 128 the same initial conditions as in the symmetric case except for $p_\psi = 5.0001$, and the
 129 remaining initial conditions are $x = y = \phi = \psi = p_x = p_y = p_z = p_\theta = 0$, $z = Z_s$,
 130 $p_\phi = 5.0$ and $\theta = 0.005$. The results are displayed in Figs. 2(a) and 2(b). Let us notice
 131 that the coordinates (x, y) are no longer fixed at the origin, nevertheless the spinning
 132 top remains stable for about the same extent of time as in the symmetric case. From
 133 now on we will work with these initial conditions for the angular velocities p_ϕ and
 134 p_ψ . The flight time of our numerical computations overcome the 900 units of times.

135 3.2 Dissipative equations

136 The dissipation terms come from two different types of motion involved in the flight
 137 of the spinning top: translation and rotation. Therefore two positive constants are
 138 needed, namely, C_T and C_R . The dissipative terms added to the Eqs. (6g)–(6i) are
 139 $-C_T p_x$, $-C_T p_y$ and $-C_T p_z$ respectively. Since the rotational velocity is very high
 140 compared with the translational velocity, we will model this friction with a quadratic
 141 term. Therefore the dissipative terms added to the Eqs. (6j)–(6l) are $-C_R p_\theta |p_\theta|$,
 142 $-C_R p_\psi |p_\psi|$ and $-C_R p_\phi |p_\phi|$ respectively. The absolute value is used in order to pre-
 143 serve the sign of the rotation velocity ensuring that all three terms act against the
 144 rotation of the spinning top. The value of the dissipation constant has been obtained
 145 by numerical calibration. Numerical simulations using $C_T = C_R = 0.1$ are displayed
 146 in Figs. 3(a) and 3(b). It can be observed that the spinning top falls after a short
 147 period of time. Figure 3(b) shows how the stable position in the (x, y) -plane is lost.

148 The z -coordinate could have a bigger variation than that of the x or y -coordinates,
 149 and then a different third dissipative constant could be introduced to add more dissi-
 150 pation in the vertical direction. Numerical simulations have been carried out using a
 151 third dissipation constant for the z -coordinate, finding that even more longer periods
 152 of time of stable flight of the spinning top are feasible.

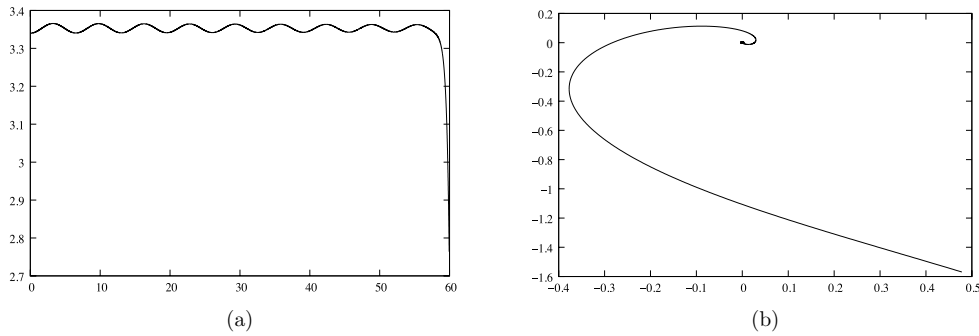


Fig. 3. (a) Time evolution of z -coordinate; (b) (x, y) -coordinates.

3.3 Forced equations

There are different strategies to force the equations of motion; they are basically of two types: electromagnetic and mechanical. Those using electromagnetic fields, which introduce torque forces into the system, have been extensively implemented in the past (see [6]). In the present effort instead, we aim to study mechanical forcing schemes, in particular, the forcing of the vertical coordinate of the position of the permanent magnetic base by small motions simulated in order to inject energy into the system.

Taking the Z -coordinate from the initial condition Z_c , we add one term to the equilibrium point Z_s , i.e. we perform the following change

$$Z_s \mapsto Z_s(1 + \beta \cos \omega t), \quad (14)$$

and refer to this perturbation as a parametric forcing.

We will analyze, locally, the effects of a parametric perturbation of the magnetic base in the Z coordinate, which will lead us to a Mathieu equation. Afterwards, we will add a dissipative term and obtain a stability diagram with an Arnold's tongue structure (see [10]).

To model a parametric perturbation of the Levitron's magnetic base, we change the equilibrium point of the system (12) by performing the transformation (14). Therefore, the linearized equation near the point $(0, Z_s)$ reads

$$\ddot{Z} + V''_{Inv}(Z_s(1 + \beta \cos(\omega t)))Z = 0. \quad (15)$$

where, from (13),

$$V''_{Inv} = -\mathcal{M}f_3(Z) = -\mathcal{M}f_0'''(Z) = -\mathcal{M} \frac{90Z^2(1 + Z^2) - 9(1 + Z^2)^2 - 105Z^4}{(1 + Z^2)^{9/2}}. \quad (16)$$

The parametric oscillation of the base is locally described by a Mathieu equation in the Z -coordinate, (15). Therefrom, we expect that the parameters β and w give rise to a stability diagram for the the Levitron's solutions with an Arnold's tongue structure.

When introducing a dissipative term to the equation we expect that the perturbation added to the magnetic base, with a suitable calibration of the amplitude and frequency, will inject energy into the system leading to a steady levitation of the spinning top for a rather long time. The parameters β and w will be found numerically since the local theoretical analysis could turn out very complicated.

181 The equations of motion (6) plus the dissipative terms introduced in Sect. 3.2
 182 provide a realistic model for the flight of the spinning top. In this section we use the
 183 forced equations as a way to simulate a small vertical motion of the magnetic base
 184 to inject energy into the system. Numerically, we will show that this results in a long
 185 period stable flight of the Levitron.

186 4 Stability of the Levitron solutions

187 We are interested in studying the non-linear stability of any solution of Eq. (6).
 188 A standard method to gain this information consists in computing the well-known
 189 maximum Lyapunov characteristic exponent (MLCE) for each orbit. For our study,
 190 it is important to use a fast method to compute the MLCE, since the variation of the
 191 flying time is very large when we change the value either of the parameters or the
 192 initial conditions of Eq. (6). Let us state that by flying time we refer to the period
 193 while the spinning top levitates in a bounded region around the fixed point. A novel
 194 method to determine the MLCE fast enough is the Mean Exponential Growth factor
 195 of Nearby Orbits (MEGNO). In this section we outline this technique but a detailed
 196 description of the MEGNO can be found for instance in [11].

197 Let us recall that the MEGNO is a fast indicator of the dynamics which is effi-
 198 cient to examine both regular and chaotic components of the phase space of a given
 199 dynamical system. Furthermore, it succeeds in revealing both the resonance structure
 200 and the location of stable and unstable periodic orbits. But herein, what interest us
 201 the most is that it provides a measure of hyperbolicity in chaotic domains which
 202 coincides with that given by the MLCE, but in a considerably shorter evolution time
 203 as already stated.

204 Consider the following equations of motion defined in $B' \subseteq M_h$

$$\dot{\mathbf{x}} = \mathbf{v}(\mathbf{x}). \quad (17)$$

205 Now, let $\varphi(t)$ denote a solution of the flow (17) corresponding to a given initial
 206 condition \mathbf{x}_0 , so that

$$\varphi(t) = \{\mathbf{x}(t; \mathbf{x}_0), \mathbf{x}_0 \in B'\}. \quad (18)$$

207 Let us introduce the definition of the Mean Exponential Growth factor of Nearby
 208 Orbits (MEGNO), $Y(\varphi(t))$, given by

$$Y(\varphi(t)) = \frac{2}{t} \int_0^t \frac{\dot{\delta}(\varphi(s))}{\delta(\varphi(s))} s ds. \quad (19)$$

209 where $\varphi(t)$ is the solution of the variational Eq. of (17)

$$\dot{\delta} = \Lambda(\varphi(t))\delta, \quad (20)$$

210 and $\Lambda(\varphi(t))$ is the Jacobian matrix of (17).

211 The MEGNO's temporal evolution can be summarized in a single expression that
 212 provides its asymptotic behavior:

$$\bar{Y}(\varphi(t)) \approx a_\varphi t + b_\varphi \quad (21)$$

213 where $a_\varphi = \sigma_\varphi/2$ and $b_\varphi \approx 0$ for chaotic motion, while $a_\varphi = 0$ and $b_\varphi \approx 2$ for stable
 214 quasiperiodic motion. Departures from the value $b_\varphi \approx 2$ indicate that φ is close to
 215 some periodic orbit, being $b_\varphi \lesssim 2$ and $b_\varphi \gtrsim 2$ for stable or near-unstable periodic
 216 orbits, respectively.

217 Let us indicate that $\hat{\sigma}_1 \equiv Y(\varphi(t))/t$ verifies

$$\hat{\sigma}_1(\varphi_q(t)) \approx \frac{2}{t}, \quad \hat{\sigma}_1(\varphi_i(t)) \approx \sigma_i, \quad t \rightarrow \infty, \quad (22)$$

218 rendering clear that, for regular motion $\hat{\sigma}_1$ converges to 0 faster than σ_1 , which
 219 vanishes at a rate $\ln t/t$, while for chaotic motion both quantities approach the positive
 220 MLCE at a similar rate.

221 4.1 Bifurcation diagram

222 We studied the flying time variation while changing the damping and perturbation
 223 parameters. We set the parameter $\mathcal{M} = 32.75367$.

With that aim we adopted for the damping parameters the values $C_T = 0.2$ and
 $C_R = 0.01$ and computed the flying time for different values of β and ω . The set of
 values of β taken for the simulations are

$$\beta = n(0.001) \quad n = 0, \dots, 2000,$$

and for each of these values of β , we took the values of the oscillation frequency

$$\omega = n(0.004) \quad n = 0, \dots, 1000,$$

224 which accounts for a total of two millions integrations. The initial conditions are
 225 the same as those used in Sect. 3.1. The initial step of integration is 0.001 and the
 226 approximation error is of the order of 10^{-14} . The stop condition used for the numerical
 227 integration is

$$|X| + |Y| + |Z - Z_s| > 2 \quad (23)$$

228 where Z_s is the equilibrium point found in previous sections. All the simulations were
 229 performed by the GPU-cluster of IIMAS-UNAM.

230 The results of these simulations are shown in Fig. 4. The vertical axis corresponds
 231 to values of β and the horizontal one to values of ω . Every point in the graph is
 232 coloured according to the value of the flight time in a logarithm scale. The largest
 233 flight time is $96u$.

234 The plot 4 looks similar to the structure of Arnold's tongues that we find in the
 235 bifurcation diagram of the nonlinear Mathieu equation. The solutions with exponen-
 236 tial growth and exponential damping have a short flying time since such solutions
 237 leave the equilibrium region in a short time and the top falls to the ground; at this
 238 point the integration has to stop. On the other hand, solutions with large flying times
 239 correspond to the cases in which a delicate equilibrium is preserved between the
 240 excitation and dissipative forces with the nonlinear behavior of Eq. (6). Figure 4
 241 shows that the accumulation of points with larger flying time are located in the re-
 242 gion given by $0 < \omega < 1.0$ and $0 < \beta < 2.0$.

243 The parametric excitation can not restore the loss of the rotational energy.
 244 Nevertheless, the stable regions in the Arnold's tongues correspond to solutions which
 245 avoid the growth of the absolute value of the following terms

$$\frac{p_\psi - p_\phi \cos \theta}{\sin^2 \theta} \quad \text{and} \quad \frac{(p_\phi \cos \theta - p_\psi)(p_\psi \cos \theta - p_\phi)}{\sin^3 \theta}, \quad (24)$$

246 when θ is close to zero. The values of $|p_\phi|$ and $|p_\psi|$ reduce their value in a monotonic
 247 fashion while the magnitude of (24) remains bounded in the stable regions on Fig. 4.

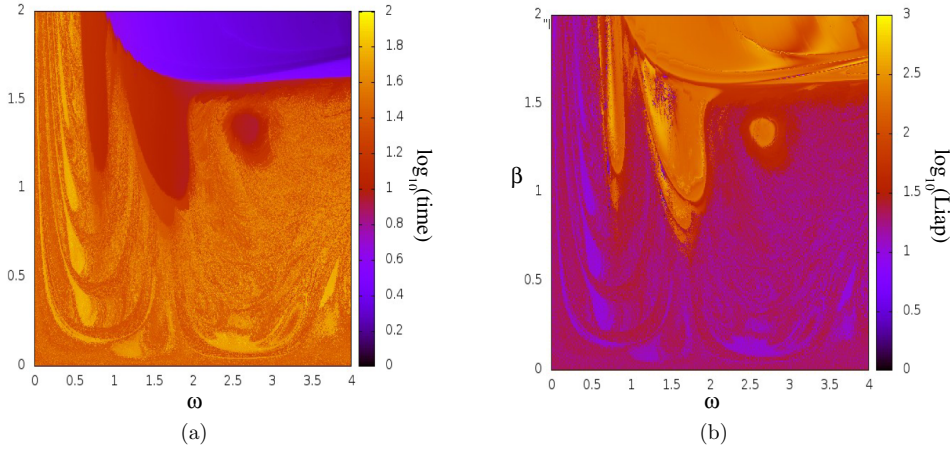


Fig. 4. (a) The axes correspond to the perturbation frequency (ω) and the perturbation amplitude (β), a) flight time is represented by colour intensity in a logarithmic scale; b) The logarithm of largest Lyapunov exponent is represented by colour intensity

248 We would like to count with a method to estimate the Levitron's flying time
 249 without having to perform the whole numerical integration until the top falls to the
 250 ground. To this end, we computed the largest Lyapunov exponent for our numerical
 251 simulations by means of the MEGNO method described in the previous section. We
 252 computed a reduced set of the variational Eq. (20). Indeed, in this case we only
 253 considered the linear equations of the position and angular variables. The reason to
 254 discard the variational equations corresponding to the momentum variables in (20) is
 255 due to the behavior of the Eq. (24). The full system (20) is very unstable when $\theta \rightarrow 0$
 256 since the matrix $\Lambda(\varphi(t))$ becomes singular in such a case.

257 We computed the bifurcation diagram of the largest Lyapunov exponent in a
 258 similar way to that used for Fig. 4, but in this case the colour code corresponds
 259 to the value of the largest Lyapunov exponent. The outcome bifurcation diagram is
 260 shown in Fig. 4b), where the value of the largest Lyapunov exponent is given in an
 261 logarithmic scale. We observe that the set of Arnold's tongues of the largest flight
 262 time in Fig. 4 matches the corresponding Arnold's tongues in Fig. 4b). Therefrom,
 263 we can conjecture that the early computation in time of the Lyapunov exponent is a
 264 good indicator that permits to predict the Levitron's flight time.

265 5 Conclusions

266 In this paper we studied the dynamics of the Levitron, in particular we were
 267 interested in determining the flying time when we added dissipation in the equa-
 268 tions of motion. In such a case the flying time is limited to $t < 23u$. In order to
 269 extend this time, we introduced a mechanical perturbation to the magnetic field of
 270 the permanent magnet, which corresponds to a parametric forcing (14). We made a
 271 systematic study of the flying time as a function of two parameters of the perturba-
 272 tion, β and ω , and obtained a detailed bifurcation diagram which is shown in Fig.
 273 4. In this diagram we can appreciate the formation of Arnold's tongues where the
 274 flying time exceeds the limit time $t < 23u$. We also analysed the stability of these
 275 solutions by means of a fast technique to compute the maximum Lyapunov exponent,
 276 the Mean Exponential Growth factor of Nearby Orbits (MEGNO). The results are
 277 displayed in Fig. 4(b) (where the stable zones correspond to values of the MEGNO

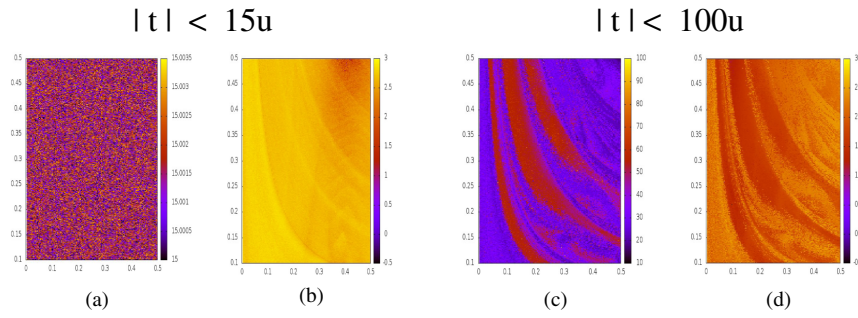


Fig. 5. Bifurcation diagrams of the parametric perturbation. ω is represented in the horizontal axes and β in the vertical axes. Figures(a) and (c) show the bifurcation diagram of the flying time where colour intensity represents the flying time; Figs.(b) and (d) show the bifurcation diagram of MEGNO; there the colour intensity represents the MEGNO value. Figures(a) and (b) are limited in time to $t < 15u$; for Figs.(c) and (d) the limit time is $t < 100u$

278 close to 2) which shows a very similar structure of Arnold's tongues as the one found
 279 in the flying time diagram.

280 In the end we concluded that the MEGNO serves as an early indicator of the
 281 stability of the solutions to the Levitron's equations. Figure 5 shows a small region
 282 of the bifurcation diagrams where the flying time was limited to $t < 15u$ (Fig. 5(a)).
 283 In this case we could not distinguish any structure similar to Fig. 4, instead the
 284 plot looks like a random distribution. However, when we increase the maximum flying
 285 time to $t < 100u$, we can appreciate the Arnold's tongues structure as can be seen in
 286 Fig. 5(c). On the other hand, in the bifurcation diagram of the Lyapunov exponent
 287 for $t < 15u$ given in Fig. 5(b), an early formation of the Arnold's tongues can be
 288 detected where MEGNO is close to the value 2. Figure 5(d) shows a clearer forma-
 289 tion of the Arnold's tongues for the MLCE diagram. In sum we can state that
 290 MEGNO allows for an early indication of stability of any solution of the Levitron
 291 equations, and the stable solutions are good candidates to have very long flying
 292 times.

293 This work was founded by FENOMECC-UNAM and CONACyT project 133036-F. We also
 294 express our gratitude to Pablo Cincotta for his invaluable help in description of MEGNO
 295 routines and Ana Perez for her assistant in the computer implementation. Finally, we would
 296 also like to thank the anonymous referee whose valuable comments have improved the pre-
 297 sentation of the paper.

298 References

- 299 1. S. Earnshaw, Trans. Cambridge Philos. Soc. 97 (1842)
- 300 2. M.V. Berry, Proc. R. Soc. London A. **452**, 1207 (1996)
- 301 3. M.D. Simon, L.O. Heflinger, S.L. Ridgway, Amer. J. Phys. **65**, 286 (1997)
- 302 4. H.R. Dullin, R.W. Easton, Phys. D. **126**, 1 (1999)
- 303 5. R.F. Gans, T.B. Jones, M. Washizu, J. Phys. D: Appl. Phys. **31**, 671, (1998)
- 304 6. A.T. Pérez, P. García-Sánchez, Amer. J. Phys. **83**, 133 (2015)
- 305 7. J.D. Jackson, *Classical Electrodynamics* 2nd edn. (Wiley, 1975)
- 306 8. L. Meirovitch, *Methods of Analytical Dynamics* (Dover Publications, 2009)

- 307 9. J. Geiser, K.F. Lüskow, R. Scheider, *Dynamical Syst.* **29**, 208 (2014)
- 308 10. D.W. Jordan, P. Smith, *Nonlinear Ordinary Differential Equations: An Introduction to*
- 309 *Dynamical Systems (Oxford Texts in Applied and Engineering Mathematics)*. 3rd edn.
- 310 (Oxford University Press, 1999)
- 311 11. P.M. Cincotta, C.M. Giordano, C. Simó, *Phys. D.* **182**, 11 (2003)

AQ: The caption from Fig. 2 have been modified, since they have been repeated? Please check is this OK?